Turbulent Thermal-Wind-Driven Coastal Upwelling: Current Observations and Dynamics

S. J. LENTZ[a]

[a] *Physical Oceanography, Woods Hole Oceanographic Institution, Woods Hole, Massachusetts*

(Manuscript received 18 March 2022, in final form 15 July 2022)

ABSTRACT: A remarkably consistent Lagrangian upwelling circulation at monthly and longer time scales is observed in a 17-yr time series of current profiles in 12 m of water on the southern New England inner shelf. The upwelling circulation is strongest in summer, with a current magnitude of ~1 cm s^{-1}, which flushes the inner shelf in ~2.5 days. The average winter upwelling circulation is about one-half of the average summer upwelling circulation, but with larger month-to-month variations driven, in part, by cross-shelf wind stresses. The persistent upwelling circulation is not wind-driven; it is driven by a cross-shelf buoyancy force associated with less-dense water near the coast. The cross-shelf density gradient is primarily due to temperature in summer, when strong surface heating warms shallower nearshore water more than deeper offshore water, and to salinity in winter, caused by fresher water near the coast. In the absence of turbulent stresses, the cross-shelf density gradient would be in a geostrophic, thermal-wind balance with the vertical shear in the along-shelf current. However, turbulent stresses over the inner shelf attributable to strong tidal currents and wind stress cause a partial breakdown of the thermal-wind balance that releases the buoyancy force, which drives the observed upwelling circulation. The presence of a cross-shelf density gradient has a profound impact on exchange across this inner shelf. Many inner shelves are characterized by turbulent stresses and cross-shelf density gradients with lighter water near the coast, suggesting turbulent thermal-wind-driven coastal upwelling may be a broadly important cross-shelf exchange mechanism.

SIGNIFICANCE STATEMENT: A remarkably consistent upwelling circulation at monthly time scales is observed in a 17-yr time series of current profiles in shallow water off southern New England. This is not the traditional wind-driven coastal upwelling; instead, it is forced by cross-shelf buoyancy (density) gradients, released by turbulent stresses in shallow water. The persistent upwelling circulation is strongest in summer, when wind and wave forcing are weak, and flushes the inner portion of the continental shelf in a few days. Consequently, this buoyancy-driven coastal upwelling is important for cooling the inner shelf and provides a reliable mechanism for cross-shelf exchange. Many inner shelves are characterized by cross-shelf density gradients and turbulent stresses, suggesting this may be a broadly important cross-shelf exchange mechanism.

KEYWORDS: Buoyancy; Coastal flows; Currents; Dynamics; Lagrangian circulation/transport; Upwelling/downwelling

1. Introduction

In classical coastal upwelling, along-shelf winds drive an offshore transport in the surface boundary layer and because of the coastal boundary, there is a compensating onshore and upward transport of subsurface water (Ekman 1905; Smith 1981; Brink 2016). Wind-driven coastal upwelling regions are among the most productive areas in the global ocean due to the upwelling of nutrient-rich subsurface waters into the euphotic zone (e.g., Falkowski et al. 1998). Observations are presented here of a different type of persistent coastal upwelling driven, not by wind stress, but by cross-shelf density (buoyancy) gradients. In a steady, linear, rotating system without turbulent stresses, a cross-shelf density gradient would be in geostrophic, thermal-wind balance with the vertical shear in the along-shelf current. Turbulent stresses allow a partial release of the cross-shelf buoyancy force that drives a cross-shelf circulation (reviewed in section 2; e.g., Garrett and Loder 1981). If density decreases toward the coast the buoyancy force drives an upwelling circulation, with offshore flow near the surface and onshore flow near the bottom (Fig. 1). This buoyancy-driven upwelling may be important over inner shelves that typically have both turbulent stresses and cross-shelf density gradients.

Martha's Vineyard Coastal Observatory (MVCO) was established over the inner shelf south of Martha's Vineyard (Fig. 2) in August of 2001 to collect long-term meteorological and oceanographic time series (Kirincich 2021). The resulting 17-yr time series of current profiles, meteorological forcing, surface gravity wave characteristics, and seawater density provide a rare opportunity to examine the characteristics and dynamics of annual and interannual current variability at an inner-shelf site. Previous observational studies focusing on daily time scales have found that cross-shelf circulations at this site are primarily driven by surface gravity waves (Lentz et al. 2008) and cross-shelf winds (Fewings et al. 2008; Horwitz and Lentz 2014). This study will show that surface gravity waves (section 4a) and cross-shelf winds (section 4d) drive cross-shelf circulations at longer time scales in a manner consistent with these previous studies. However, the dominant

Denotes content that is immediately available upon publication as open access.

Corresponding author: S. J. Lentz, slentz@whoi.edu

DOI: 10.1175/JPO-D-22-0063.1

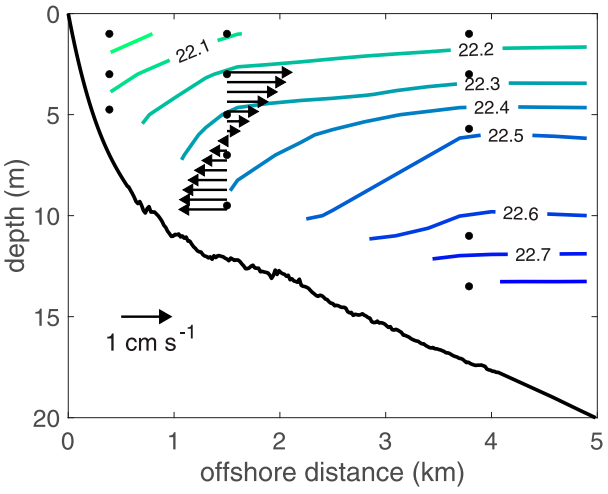

FIG. 1. Cross-shelf section extending 5 km offshore showing average summer (April–September) density structure during SWWIM and the average summer cross-shelf current profile (depth dependent) from the 17-yr ADCP time series at the 12-m site. Black dots indicate temperature–conductivity sensor positions. Densities from the 27-m site, 11 km offshore, are used in contours but are not shown.

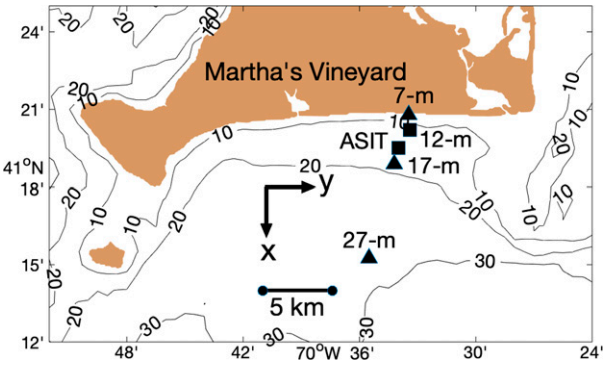

FIG. 2. Map of the inner shelf south of Martha's Vineyard showing 17-yr MVCO 12-m and Air–Sea Interaction Tower (ASIT) sites (squares), 3-yr SWWIM sites (triangles) where temperature–conductivity chains were deployed, and the coordinate frame.

cross-shelf circulation at monthly time scales is a remarkably consistent turbulent thermal-wind (buoyancy)-driven coastal upwelling that is strongest in summer when wind and surface gravity wave forcing are weakest (sections 4b and 4c).

2. Turbulent thermal-wind balance

In a geostrophic flow with a lateral (cross shelf) density gradient, the thermal-wind balance

$$-f\frac{\partial v}{\partial z}=\frac{g}{\rho_o}\frac{\partial \rho}{\partial x} \tag{1}$$

is between the Coriolis force associated with the vertical shear in the along-shelf current v and the buoyancy force associated with the cross-shelf density gradient $\partial\rho/\partial x$. Here z is positive upward, x is positive offshore (Fig. 2), f is the Coriolis frequency, g is gravitational acceleration, and ρ_o is a reference density.

The thermal-wind balance is steady, linear, and inviscid; there are no turbulent stresses. However, over shallow inner shelves, turbulent stresses often extend throughout the water column (e.g., Kirincich 2013). To illustrate the key features of a turbulent thermal-wind balance, consider steady, linear dynamics with no along-shelf variations and assume there is a cross-shelf density gradient that is independent of depth (e.g., Garrett and Loder 1981; Chen and Chen 2017). The cross-shelf and along-shelf momentum balances are

$$-fv=-g\frac{\partial \eta}{\partial x}+\frac{g}{\rho_o}\frac{\partial \rho}{\partial x}z+\frac{\partial}{\partial z}A_v\frac{\partial u}{\partial z} \quad \text{and} \tag{2}$$

$$fu=\frac{\partial}{\partial z}A_v\frac{\partial v}{\partial z}. \tag{3}$$

Here η is the sea level variation and A_v is a turbulent eddy viscosity. If there are no turbulent stresses ($A_v = 0$), Eq. (2) reduces to a geostrophic balance that includes the thermal-wind balance in Eq. (1) and, from Eq. (3), there is no cross-shelf circulation. If there is no cross-shelf density gradient ($\partial\rho/\partial x = 0$), then, for an applied wind stress, Eqs. (2) and (3) reduce to the classic coastal Ekman (1905) response that includes a barotropic, geostrophic along-shelf current.

Starting from a thermal-wind balance and applying turbulent mixing causes a reduction in the along-shelf current shear and hence an unbalanced portion of the buoyancy force. This unbalanced buoyancy force accelerates a cross-shelf circulation until the cross-shelf turbulent stress divergence in Eq. (2) balances the difference between the two components of the thermal-wind balance. Equation (3) indicates that there may be a cross-shelf circulation driven by the turbulent stress divergence associated not only with wind stress and bottom stress, but also the eddy viscosity acting on the thermal-wind shear.

These features of the response are clearly seen in an analytic solution to Eqs. (2) and (3) forced by an along-shelf wind stress derived by Chen and Chen (2017). They assume an imposed vertically uniform cross-shelf density gradient and eddy viscosity $A_v = \kappa u_* D/6$, where $\kappa = 0.4$ is the von Kármán constant, $u_* = (|\tau^s|/\rho)^{1/2}$ is the shear velocity associated with the wind stress, and D is the water depth. They also assume that the cross-shelf velocity is weak and hence does not contribute to the bottom stress. With these assumptions, the ageostrophic velocity is

$$u_a+iv_a=\left(\frac{\tau^{sy}D}{\rho A_v}+\frac{gD}{\rho f}\frac{\partial \rho}{\partial x}\right)\times\left\{\frac{(1+i)}{2\tilde{D}}\frac{\cosh[(1+i)(\tilde{z}+\tilde{D})]-\cosh[(1+i)(\tilde{z})]}{\sinh[(1+i)\tilde{D}]}\right\}, \tag{4}$$

where τ^{sy} is the along-shelf wind stress, $D_E=\sqrt{2A_v/f}$ is the Ekman depth, $\tilde{z}=z/D_E$, and $\tilde{D}=D/D_E$. The first two terms on the right-hand side are velocity scales associated with the wind-driven shear and the geostrophic shear, both times the

water depth. The remaining term (in curly braces) only depends on $\tilde{z}$ and $\tilde{D}$, and determines the vertical structure of the current and the strength of the Ekman response depending on whether the water depth D is large or small relative to the Ekman depth D_E. Note that the along-shelf wind stress drives a crosswind Ekman circulation and also imposes a turbulent stress that determines the strength of the eddy viscosity A_v and hence the Ekman depth D_E. The cross-shelf velocity is entirely ageostrophic, $u = u_a$, since there is no along-shelf pressure gradient in this idealized case. If the wind-driven shear is much larger than the thermal-wind shear, the cross-shelf circulation is driven by the wind stress and Eq. (4) reduces to the classic coastal Ekman response (Ekman 1905). If the thermal-wind shear is large relative to the wind-driven shear, then the cross-shelf circulation is driven by the buoyancy force rather than the wind stress. Chen and Chen (2017) show a great example of this, where a downwelling-favorable wind, acting on a buoyant coastal current, drives an upwelling circulation in shallow water because the buoyancy driven thermal-wind shear exceeds the wind-driven shear and has the opposite sign. In summary, the three components required to generate a turbulent-thermal-wind-driven cross-shelf (cross-isopycnal) circulation are a 1) rotating system, 2) buoyancy gradient, and 3) turbulent stress.

The notion of a turbulent thermal-wind balance (McWilliams et al. 2015) goes back at least to the early 1970s when Heaps (1972) proposed it as an explanation for density currents in the Irish Sea. A number of subsequent studies examined tidal mixing fronts in the context of a turbulent thermal-wind balance (e.g., James 1978; Loder and Wright 1985) including a comprehensive theoretical treatment by Garrett and Loder (1981). These dynamics have also been used to explain the presence of an upwelling circulation in a buoyant plume driven by downwelling-favorable winds (Moffat and Lentz 2012; Chen and Chen 2017) and the cross-frontal circulation in open ocean fronts (e.g., Nagai et al. 2006; Ponte et al. 2013) and filaments (Gula et al. 2014; McWilliams et al. 2015).

3. Measurements and analyses

a. Site, measurements, and processing

MVCO includes a cabled underwater node 1.5 km offshore in 12 m of water that has been operational since August 2001. At the node there is an RDI broadband acoustic Doppler current profiler (ADCP) sampling at 2 Hz, resulting in 20-min averages of both current profiles and surface gravity wave directional spectra (available at https://www.whoi.edu/mvco/). Reliable ADCP current profiles extend from 2.5 to 10 m above the bottom. There is also a single temperature–conductivity sensor deployed about 2 m above the bottom on the pedestal supporting the ADCP.

Surface gravity wave Stokes drift velocity profiles are estimated from the 20-min wave directional spectra following Kenyon (1969). The directional spectra consist of a single wave direction at each frequency, that is, no directional spread, and wave directions are uncertain for wave periods shorter than 3 s. The MVCO Stokes velocity estimates were compared with estimates from a 5-beam ADCP sampling at 4 Hz deployed nearby for ~5 months in 2014 that provided more accurate estimates of the wave directional spectra, including directional spread. The wave directional spectra from the MVCO ADCP underestimate the Stokes velocity by about 25% relative to the 5-beam ADCP because of the lower cutoff frequency but overestimate the Stokes velocity by about 40% as a result of not accounting for directional spread in the spectra. In both cases the time series are highly correlated. [See Webb and Fox-Kemper (2015) for a thorough discussion of the challenges in estimating accurate Stokes velocities from directional spectra.] Here the Stokes velocity is calculated from the MVCO wave directional spectra without correcting for contributions from higher frequencies or wave directional spread. Lagrangian currents are estimated as the sum of the estimated Stokes velocities u^S and the measured Eulerian velocities u^E from the ADCP (i.e., $u^L = u^S + u^E$).

Meteorological measurements have been made at the MVCO shore mast since 2001 and an Air–Sea Interaction Tower (ASIT) 2.8 km offshore (Fig. 2) since 2004. Wind stress at ASIT is estimated from these meteorological measurements using the Coupled Ocean–Atmosphere Response Experiment (COARE) 3.5 bulk algorithm (Edson et al. 2013).

Depth-average currents are estimated by transforming the current profiles to a water-depth normalized uniform grid and then, for simplicity, averaging the currents without extrapolating to the surface or bottom. (Results are essentially the same if currents are linearly extrapolated to the surface and bottom.) Monthly (calendar) averages are estimated from the 20-min samples. Currents are detided (Pawlowicz et al. 2002) prior to estimating monthly averages. Currents and wind stresses are rotated into a coordinate frame aligned with the principal axes of the monthly depth-average Lagrangian currents. Cross shelf (x, u) is positive offshore and along shelf (y, v) is positive eastward (94.5° clockwise from true north) (Fig. 2).

b. Estimation of the cross-shelf density gradient

A key element of the turbulent thermal-wind balance is the cross-shelf density gradient. Direct measurements of the cross-shelf density gradient are only available during a 3-yr period (October 2006–February 2010) during the Stratification, Wind and Waves on the Inner Shelf field program (SWWIM; Horwitz and Lentz 2014) when temperature–conductivity moorings, with typically 2–3-m vertical spacing between sensors, were deployed along a cross-shelf transect in water depths of 7 m (0.4 km offshore), 12 m (MVCO site, 1.5 km), 17 m (3.8 km), and 27 m (11.1 km) (Fig. 1). Cross-shelf density gradients spanning the 17-yr time series are estimated by assuming that density variations over 48-h periods are primarily driven by the depth-average tidal currents advecting the cross-shelf density gradient past the 12-m site; that is, $\partial\rho/\partial t \approx u^L_{\rm da}\partial\rho/\partial x$ (e.g., Brink et al. 2009). Daily values of $\partial\rho/\partial x$ are estimated as the linear regression slope between the depth-average Lagrangian cross-shelf current $u^L_{\rm da}$ and $\partial\rho/\partial t$ estimated as a finite difference from the 20-min samples taken 2 m above bottom (mab). The regression analysis is over 2 days periods that included a half-day overlap with

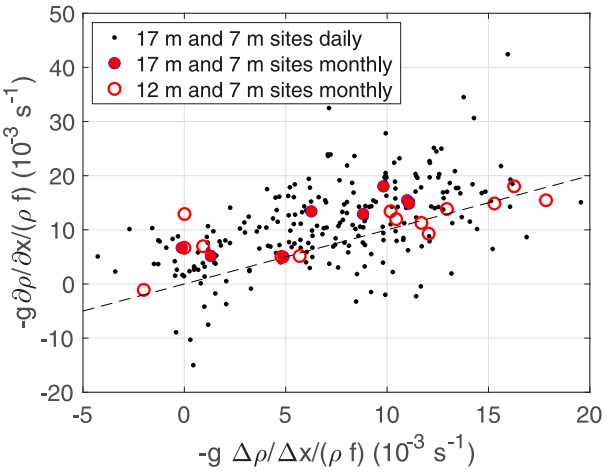

FIG. 3. Comparison of thermal-wind shear estimated from finite differences between moored density measurements in 7, 12, and 17 m of water during the 3-yr SWWIM study (x axis) and estimated from density and cross-shelf velocity measurements at the 12-m MVCO site as a linear regression slope assuming $\partial\rho/\partial t \approx u^L_{\rm da}\partial\rho/\partial x$.

the previous and following day. This analysis resulted in 115 monthly averages (~9.5 yr) estimated from the daily values. This estimate of $\partial\rho/\partial x$ clearly makes a number of strong assumptions, notably that, at tidal time scales, vertical mixing, vertical advection, and along-shelf advection of density are, on average, small relative to cross-shelf advection.

The cross-shelf density gradient estimates are compared with finite differences between density measurements at the same depth at the 7- and 17-m (13 months) and the 7- and 12-m (24 months) SWWIM sites. At daily time scales, the correlation between the SWWIM quasi-centered finite-difference estimates (7- and 17-m sites) and the 12-m site advective estimates is 0.54 with a regression slope of 0.90 ± 0.19 (95% confidence interval) (Fig. 3, black dots). For monthly averages, the correlations are 0.86 for the 7-to-17-m difference and 0.78 for the one-sided 7-to-12-m site difference (Fig. 3, red circles). The corresponding regression slopes are 0.74 ± 0.43 and 1.00 ± 0.50, respectively. The advective estimates reproduce the annual cycle of $\partial\rho/\partial x$ observed during SWWIM (see section 4c, Fig. 6b). This comparison indicates that the monthly averaged $\partial\rho/\partial x$ estimates based on $\partial\rho/\partial t \approx u^L_{\rm da}\partial\rho/\partial x$ are reasonable.

c. *Numerical model*

To provide further insight into the relationship between the observations and the turbulent thermal-wind forcing, an unstratified, steady, linear one-dimensional numerical model is used [see Lentz (1995) for a complete description]. The model solves Eqs. (2) and (3) for an applied surface wind stress and assuming no flow at the bottom. The eddy viscosity depends on the surface and bottom stresses with a vertical structure proposed by McWilliams and Huckle (2006) based on results from a large-eddy simulation model. For the shallow 12-m site forced by an along-shelf wind stress greater than 0.002 N m^{-2}, turbulence extends throughout the water column in the model and the eddy-viscosity profile is parabolic with a maximum value at middepth of $\kappa u_* D/4$ (D = 12 m). The model is forced to have a two-dimensional current structure, which satisfies the constraint of no cross-shelf transport at the coast and no along-shelf variations in the currents, by finding the barotropic, cross-shelf pressure gradient that forces the net cross-shelf transport (depth-average current) to be zero. The model has 1001 grid points in the vertical with logarithmic spacing near the boundaries. This model differs from the analytic model in Eq. (4) [developed by Chen and Chen (2017)] primarily in the inclusion of a more realistic eddy viscosity profile rather than a vertically uniform eddy viscosity.

The steady model is forced by the daily-averaged wind stress and does not include the strong tidal currents at MVCO. Scully et al. (2018) estimated an average z_o = 0.0014 m in the vicinity of MVCO from direct covariance stress estimates that included tidal currents. In the model, an enhanced hydrodynamic roughness of z_o = 0.055 m is imposed to account for tidal current and surface gravity wave contributions (Lentz 2022) to bottom stress not explicitly present in the daily averages. For the turbulent thermal-wind simulations the daily cross-shelf density gradient is assumed to be vertically uniform and is imposed as in Eq. (2). The model is diagnostic, at best, since the cross-shelf density gradient is prescribed and the model neglects stratification influences on vertical mixing (see discussion section 5d). The model is only intended to demonstrate consistency between the proposed dynamics given by Eqs. (2) and (3) and the observations (section 4c).

4. Results

The dependence of the depth-average Eulerian cross-shelf velocity on the surface-gravity-wave-driven Stokes velocity is considered in section 4a. The subsequent focus is on the characteristics of the Lagrangian cross-shelf current profiles (section 4b), and the roles of turbulent thermal wind (section 4c) and cross-shelf wind stress (section 4d) in driving the depth-dependent cross-shelf circulation. In some cases, summer (April–September) and winter (October–March) are examined separately. The 12-m site is intermittently (tidal time scales) stratified in summer and unstratified, or weakly stratified in winter.

a. *Depth-average cross-shelf currents and surface gravity wave forcing*

Monthly mean depth-average currents at MVCO are strongly polarized along shelf (Lentz 2022). The depth-averaged Eulerian cross-shelf current $u^E_{\rm da}$ standard deviation (0.3 cm s^{-1}) is one-eighth of the along-shelf current standard deviation (2.4 cm s^{-1}). At monthly time scales the depth-averaged Eulerian cross-shelf current is almost always offshore (positive) and less than 1.5 cm s^{-1}, with a mean of 0.5 cm s^{-1} (Fig. 4a, blue circles and line). Surface gravity waves are largest in fall and winter, occasionally exceeding 4 m at the 12-m site. The surface gravity waves almost always propagate northward (onshore), with wind waves (periods 4–8 s) over a broad range of directions (from −60° to 60°T, where T indicates true north) and swell (periods of 8–20 s) over a narrower range of directions

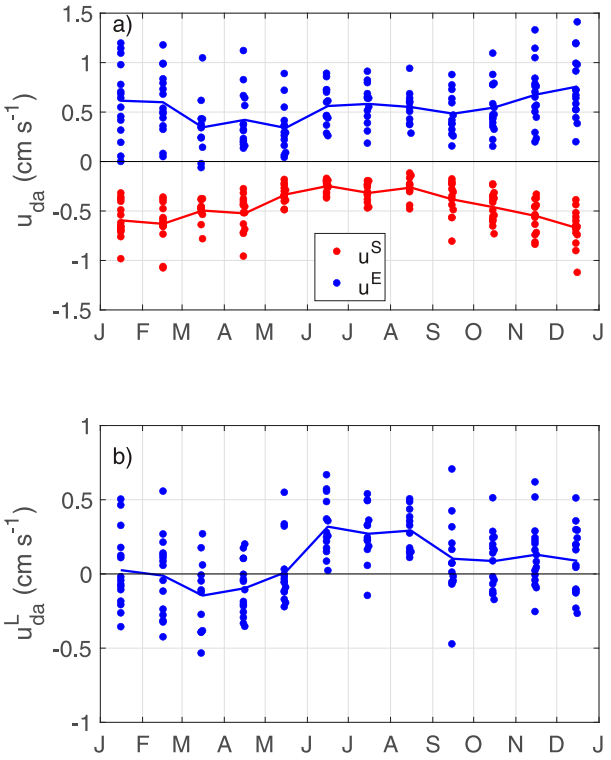

FIG. 4. Annual variation of monthly averages of the (a) depth-average Eulerian and Stokes cross-shelf currents and (b) depth-average Lagrangian cross-shelf current (positive offshore) at the MVCO 12-m site. Dots are individual months, and lines are average annual variation.

(from −30° to 20°T). The resulting depth-averaged cross-shelf Stokes velocities (u^S_{da}) are always onshore at monthly time scales, with a mean of −0.5 cm s^{-1} (Fig. 4a, red line) and larger magnitudes in winter relative to summer. Depth-average Stokes cross-shelf velocities are approximately equal in magnitude but opposite in direction to the depth-averaged Eulerian cross-shelf velocities (correlation −0.54; regression slope −0.79 ± 0.19). Consequently, the depth-averaged Lagrangian cross-shelf current ($u^L_{da} = u^S_{da} + u^E_{da}$) is typically less than 0.5 cm s^{-1} (Fig. 4b) with a mean near zero (0.09 cm s^{-1}) and a standard deviation of 0.26 cm s^{-1}. The depth-average Lagrangian cross-shelf currents are not obviously different from zero given the uncertainties in the Stokes velocities, the depth averaging, and the current measurements. In summary, at monthly time scales there is an offshore depth-average Eulerian current that is equal in magnitude and opposite in direction to the onshore, depth-average Stokes current, consistent with previous inner-shelf studies focusing on daily time scales (Lentz et al. 2008; Kirincich et al. 2009). The following sections focus on the depth-dependent (depth-average removed), Lagrangian cross-shelf current profiles.

b. *Cross-shelf current profiles*

The monthly-averaged, depth-dependent, Lagrangian cross-shelf current profiles are almost always an upwelling circulation, with offshore flow in the upper half of the water column and onshore flow in the lower half of the water column (Figs. 5 and 6a). Summer (April–September) current profiles are remarkably consistent both month to month and year to year (Figs. 5a and 6a).

During the summer, average cross-shelf currents at 3 m below the surface are offshore at 1.4 cm s^{-1} with a standard deviation of 0.27 cm s^{-1} (red symbols and line in Fig. 6a) and at 3 m above the bottom are onshore at 1.0 cm s^{-1} with a standard deviation of 0.17 cm s^{-1} (blue symbols and line in Fig. 6a). The average winter cross-shelf current profile is a weaker upwelling circulation (one-half of the summer values) but with a broader range of variability (2 times the summer standard deviations) (Fig. 5b) and occasional weak downwelling circulation in November and December (Fig. 6a). The monthly, depth-dependent part of the Stokes cross-shelf velocity magnitudes are less than 10% of the depth-dependent part of the Eulerian cross-shelf velocity magnitudes. Consequently, the depth-dependent Eulerian current profiles are similar to the Lagrangian current profiles in both summer and winter.

c. *Turbulent thermal-wind-driven cross-shelf circulation*

The annual cycle of the cross-shelf circulation is consistent with turbulent thermal-wind forcing. The three components of turbulent thermal-wind-driven coastal upwelling (the cross-shelf circulation, the cross-shelf density gradient, and the vertical shear in the along-shelf current), exhibit similar annual cycles (Fig. 6). The thermal-wind shear (cross-shelf buoyancy gradient) is on average weakly negative in January, increasing in magnitude through the late winter to an approximately constant maximum of −0.01 s^{-1} from April through September (Fig. 6b). The thermal-wind shear magnitude decreases rapidly in the fall to near-zero values in November and December, with small positive values in many years. The vertical shear in the along-shelf current (Fig. 6c) and the cross-shelf circulation (Fig. 6a) exhibit the same pattern. In particular, there is a persistent upwelling circulation throughout the year, except in November and December when the cross-shelf circulation, cross-shelf buoyancy gradient, and along-shelf velocity shear are all weak and occasionally reverse sign. Consistent with a turbulent thermal-wind balance the along-shelf current shear is smaller than the thermal-wind shear with a few exceptions (Fig. 7). The imbalance between these two terms is consistent with the presence of a persistent upwelling circulation (Fig. 6a) and a corresponding turbulent stress divergence [Eq. (2)].

The annual cycle of the cross-shelf circulation (Fig. 6a) is not consistent with along-shelf and cross-shelf wind stresses that would both force stronger upwelling circulations in the winter, when monthly wind stresses are consistently eastward and, on average, weakly offshore (Fig. 8). In summer, both along-shelf and cross-shelf wind stresses are weak with near zero monthly means.

Equation (4) indicates that the cross-shelf circulation depends on both the wind-driven turbulent stress and the turbulent stress associated with the geostrophic shear, with the eddy-viscosity determined by the wind stress. The wind-driven

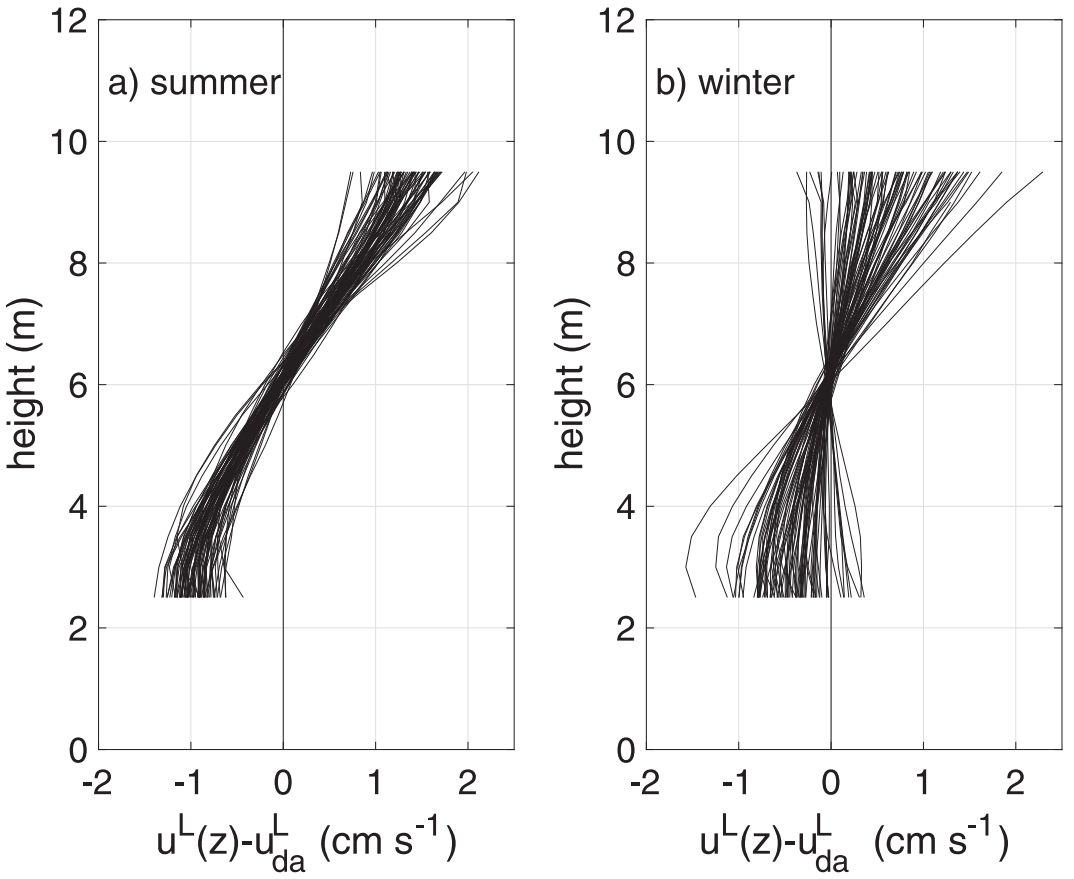

FIG. 5. All monthly Lagrangian cross-shelf current profiles (depth-average removed) for (a) summer (April–September; 82 profiles) and (b) winter (October–March; 90 profiles). Positive currents are offshore.

shear is less than 10% of the geostrophic shear in summer, but similar in magnitude in winter. Monthly averages of the vertical structure term [curly braces in Eq. (4)] at 3 m below surface range from 0.06 to 0.12 with a mean of 0.09. If one assumes that the wind-driven shear term is small relative to the thermal-wind shear and the nondimensional vertical structure term is approximately constant, the cross-shelf circulation should be proportional to the thermal-wind shear. Consistent with these assumptions the observed upwelling circulation is correlated with the geostrophic shear velocity scale (correlation 0.75 in upper and lower water column] and has roughly the expected magnitude (Fig. 9, open circles). Removing the cross-shelf wind-driven response (see following section) increases the correlations to 0.85 (Fig. 9, filled circles).

The diagnostic numerical model described in section 3c provides additional confirmation that the observed cross-shelf circulation is due to a turbulent thermal-wind balance. The model is forced by the observed daily-averaged along-shelf wind stresses and the estimated daily cross-shelf density gradients are imposed. Monthly averages of the model cross-shelf currents are correlated with the observed cross-shelf currents (correlations of ~0.8 in the upper and lower water column) and have about the same magnitudes (Fig. 10a). Setting the cross-shelf density gradient to zero in the model results in cross-shelf currents that are much smaller than the observed cross-shelf currents (Fig. 10b). In contrast, imposing the estimated cross-shelf density gradient with zero along-shelf wind stress and an eddy viscosity profile assuming a constant $u^b_* = 0.24\,\mathrm{cm\,s^{-1}}$ results in model cross-shelf currents that are very similar to both the observations and the model forced by the observed along-shelf wind stress (Fig. 10c). (The constant u^b_* is the average from the daily bottom stresses). The analytic model in Eq. (4) yields similar results but with slightly stronger cross-shelf circulations than either the diagnostic model or the observations (not shown). The agreement between Figs. 10a and 10c indicates that at monthly time scales the along-shelf wind stress does not substantially alter the monthly cross-shelf current profiles. Comparison of Figs. 10a and 10b highlights the key result of this study, that the presence of a cross-shelf density gradient has a profound impact on exchange across the inner shelf.

To gain further insight into the turbulent thermal-wind response, the dependence of the upwelling circulation on the along-shelf wind stress and cross-shelf density gradient is examined using the diagnostic model (Fig. 11). For a constant along-shelf wind stress, the dependence of the cross-shelf circulation on the thermal-wind shear (cross-shelf density gradient) is nearly linear, with a stronger upwelling circulation

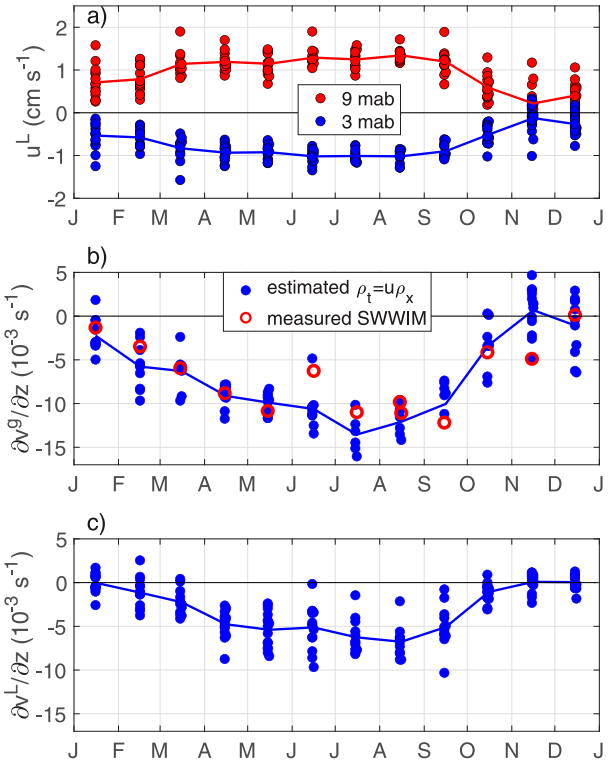

FIG. 6. Monthly averages of (a) the near-surface (red) and near-bottom (blue) cross-shelf currents (positive offshore), (b) the thermal-wind shear associated with the cross-shelf density gradient [$\partial v^g/\partial z = -(g\partial\rho/\partial x)/(\rho_o f)$], and (c) along-shelf current shear. Lines indicate average annual variation.

(current at 2 m below the surface) for the weaker summer wind stress (Fig. 11a), which is consistent with the observed response (Fig. 9).

In contrast, for a constant cross-shelf density gradient, the dependence of the cross-shelf circulation on the wind stress is

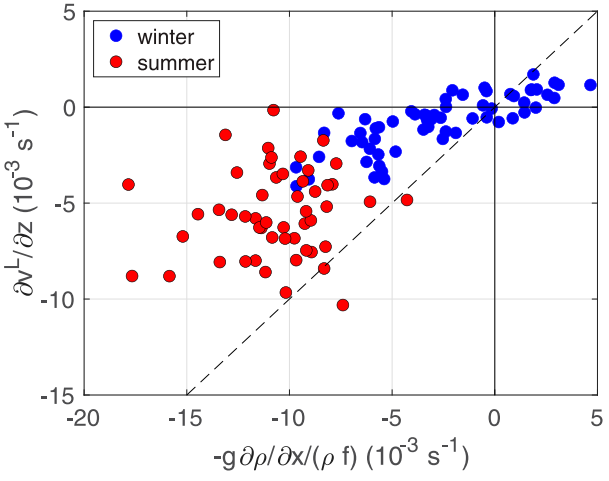

FIG. 7. Relationship between monthly thermal-wind shear and along-shelf current shear.

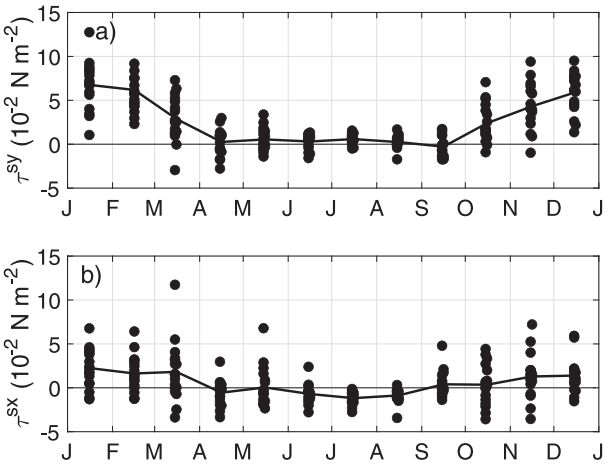

FIG. 8. Monthly averages of the (a) along-shelf (positive eastward) and (b) cross-shelf (positive offshore) wind stresses. Lines indicate average annual variation.

not linear (Fig. 11b). If there is no cross-shelf density gradient (Fig. 11b, black line) the upwelling/downwelling circulation is symmetric for positive/negative along-shelf wind stresses and nearly independent of the wind stress for magnitudes greater than 0.002 N m^{-2}. This is because the tendency for a stronger wind stress to drive a stronger cross-shelf circulation is roughly balanced by the tendency for the enhanced turbulent mixing (eddy viscosity) associated with the wind stress to decrease the Ekman response (cross-shelf circulation) in shallow water. A constant, positive cross-shelf density gradient results in an asymmetric response to the wind stress, with an enhanced upwelling circulation for small wind stress magnitudes (Fig. 11b, red and blue lines). At large wind stress magnitudes, the cross-shelf circulation becomes weakly dependent on the wind stress magnitude because of the enhancement of the turbulent mixing (eddy viscosity). For a larger cross-shelf density gradient (Fig. 11b, red line), there is an upwelling circulation even when the wind stress is downwelling favorable, as noted previously (e.g., Chen and Chen 2017).

This analysis provides an explanation for why the turbulent thermal-wind-driven upwelling at MVCO is stronger in summer than in winter, even though upwelling favorable along-shelf wind stresses are stronger and more persistent in winter. In summer, the combination of a larger cross-shelf density gradient and weaker wind stresses both contribute to drive a stronger upwelling circulation. In winter, the stronger upwelling-favorable wind stresses actually reduce the upwelling circulation, in addition to the weaker cross-shelf density gradient.

d. Cross-shelf circulation driven by cross-shelf wind stress

Previous studies have shown that cross-shelf wind stresses drive substantial cross-shelf circulations at this site on time scales of days, with downwind currents in the upper third of the water column and upwind currents in the lower two-thirds of the water column (Fewings et al. 2008; Horwitz and Lentz 2014). Theory, numerical modeling, and observations (Tilburg 2003; Lentz and Fewings 2012) indicate that the cross-shelf

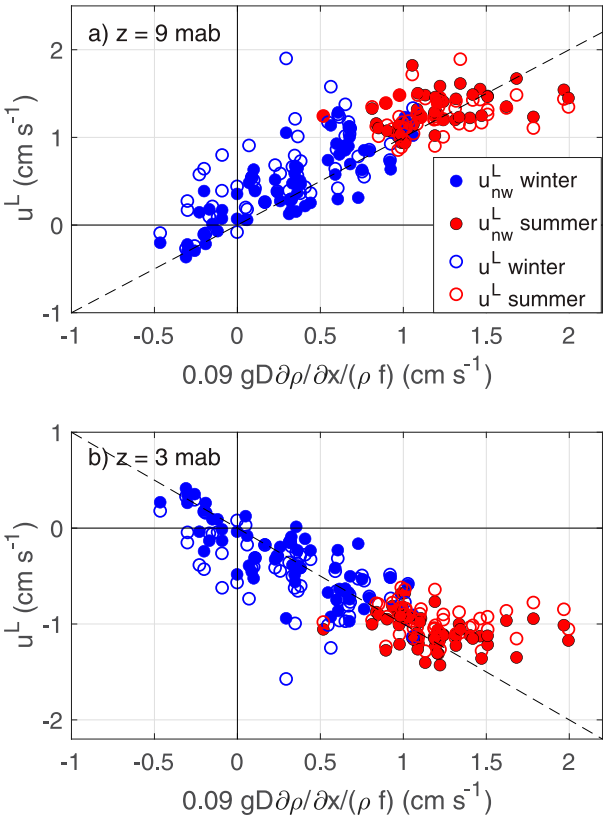

FIG. 9. Observed Lagrangian cross-shelf currents at (a) 9 and (b) 3 mab vs the geostrophic shear velocity from Eq. (4). The coefficient of 0.09 is the mean value of the real part of the term in curly braces in Eq. (4). Open circles are complete cross-shelf current, and filled circles are with cross-shelf wind response removed. The dashed line has a slope of 1 or −1.

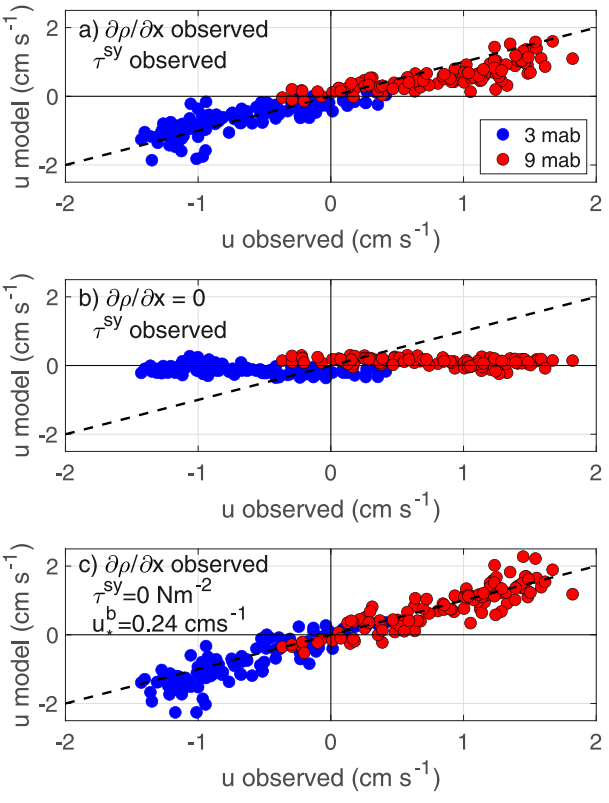

FIG. 10. Diagnostic model vs observed cross-shelf current at 3 and 9 mab forced with (a) observed along-shelf wind stress and cross-shelf density gradient, (b) with observed along-shelf wind stress but cross-shelf density gradient set to zero, and (c) estimated cross-shelf density gradient but zero along-shelf wind stress and a constant u^b_* based on daily bottom stress.

circulation driven by the cross-shelf wind stress scales with u^{sx}_*, the cross-shelf component of the shear velocity [$\sqrt{(|\tau^s|/\rho)}e^{i\theta}$, where θ is the orientation of the wind stress]. To determine whether the cross-shelf wind stress makes an observable contribution to the cross-shelf circulation at monthly time scales, monthly averaged shear velocities are estimated from the 20-min wind stresses and compared with the cross-shelf velocities. To isolate the relatively weak response to the cross-shelf wind stress, the stronger turbulent thermal-wind-driven response, discussed in the previous section, is removed using a linear regression of the cross-shelf density gradient on the cross-shelf current at each depth (e.g., Fig. 9, open circles).

For comparison with the observations, the model described in section 3c was run for cross-shelf wind stresses ranging from 0.02 to 0.12 N m^{-2} (no along-shelf wind stress or cross-shelf density gradient). The model cross-shelf currents scale with u_* so that the profiles essentially collapse onto a single curve with downwind flow in the upper third of the water column and opposing upwind flow in the lower two-thirds of the water column (Fig. 12, model profiles).

At monthly time scales the cross-shelf current fluctuations are correlated with u^{sx}_* (e.g., Fig. 12, inset). Correlations are 0.5–0.73 in the lower half of the water column but small in the vicinity of the zero crossing (as expected). In winter, the regression slopes between u^L and u^{sx}_* (Fig. 12, blue circles) exhibit almost exactly the same vertical structure as the model profiles (Fig. 12, blue lines). The observed summer current response to cross-shelf wind stresses (Fig. 12, red circles) is less sheared than the observed winter response or the model response, possibly due to the weak onshore winds (Fig. 8b) reducing the stratification (Fig. 1) (Horwitz and Lentz 2014). Thus, the cross-shelf wind stress accounts for some of the variability in the monthly cross-shelf circulation, particularly in winter when the cross-shelf wind stress variability is larger (Fig. 8b). However, the cross-shelf wind stress does not account for most of the variance in the monthly cross-shelf circulation. This is evident in Fig. 9, where the difference between including (open circles) or excluding (closed) the cross-shelf wind response is small. The cross-shelf wind stress primarily leads to a slightly stronger upwelling circulation in winter due to offshore wind stresses (Fig. 8b). The anomalously large cross-shelf circulation (Fig. 9a, largest open circle) was due to exceptionally strong offshore winds during a sequence of northeaster storms in March 2018 (Fig. 8b).

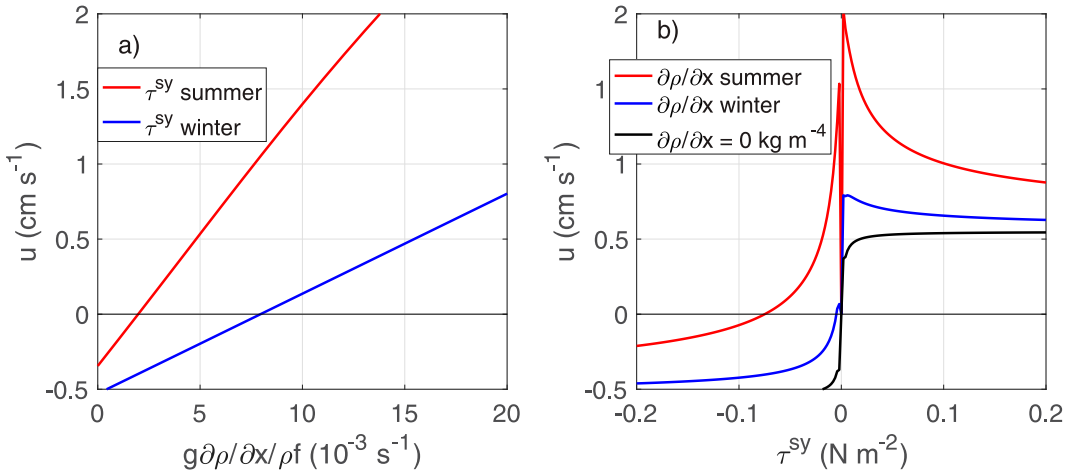

FIG. 11. Dependence of cross-shelf current at 3 m below surface on (a) the thermal-wind shear for mean summer and winter along-shelf wind stresses and (b) the along-shelf wind stress for mean summer and winter cross-shelf density gradients and no cross-shelf density gradient. Positive currents are an upwelling circulation. In (b), when the wind stress is zero, there is no turbulent stress, and consequently the cross-shelf circulation is zero, as noted previously in discussing Eqs. (2) and (3).

5. Discussion

a. *Limitations of analyses*

The MVCO observations indicate that current variability at time scales of hours to days tends to conceal the relatively weak turbulent thermal-wind-driven coastal upwelling circulation that emerges so clearly at monthly time scales (Fig. 5). For daily averages, the correlation between the observed cross-shelf circulation (3 m below surface or 3 mab) and the cross-shelf density gradient estimate is ~0.35 (significant at the 95% confidence level) as compared with 0.75 for monthly averages. The correlation exceeds 0.5 for time scales of a week or longer. Inaccuracies in the observations and estimation of terms, most notably the indirect estimate of the cross-shelf density gradient (Fig. 3), undoubtedly contribute to the weaker relationship at daily time scales. Previous studies have shown that at daily time scales cross-shelf winds (e.g., Fewings et al. 2008; Horwitz and Lentz 2014) and inner-shelf eddies (Kirincich 2016; Kirincich and Lentz 2017) are important at this site and cross-shelf flows associated with transient rip currents are probably important closer to the surfzone (e.g., Hally-Rosendahl et al. 2014). Additionally, buoyancy driven flow will be more transient, and tides and daily variations in surface heat flux may be more important (e.g., Ulloa et al. 2018; Grimes et al. 2020).

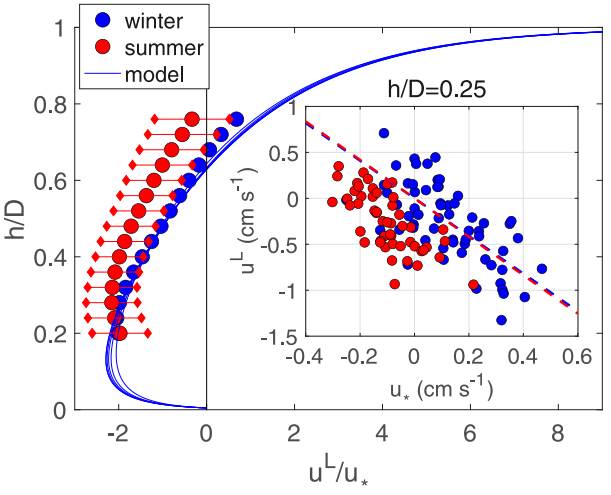

FIG. 12. Linear regression coefficients between u^L and u_* as a function of normalized height above the bottom for winter and summer. Lines are model response for $0.02 \le \tau^{sx} \le 0.12$ N m^{-2} in 0.01 N m^{-2} increments showing how normalizing by u_* collapses the model output to essentially one line. The inset shows a scatterplot of u^L vs u_* at normalized height of 0.25 for winter (blue) and summer (red). The 95% confidence intervals for the summer regressions slopes are shown; confidence intervals for the winter regression slopes are smaller.

The dynamics [Eqs. (2) and (3)] and the analytic and diagnostic models are intentionally simple to focus on the key features of the turbulent thermal-wind response. In the cross-shelf momentum balance, estimates of $\partial u/\partial t$ and $u\ \partial u/\partial x$ from the 20-min samples at the 12-m site (using distance to coast for the cross-shelf gradient) or directly from the SWWIM moorings are two orders of magnitude smaller than the terms in Eq. (2) at monthly time scales (an order of magnitude smaller at daily time scales). Scaling suggests the $v\partial u/\partial y$ term is similarly small unless the along-shelf scale of the cross-shelf velocity gradient is much less than 1 km. In contrast to the cross-shelf momentum balance, some of the neglected terms in the along-shelf momentum balance are not small. At monthly time scales, the along-shelf acceleration $\partial v/\partial t$ is negligible and the nonlinear terms $u\partial v/\partial x$ and $v\partial v/\partial x$ are ~10% of the terms in Eq. (3) (Lentz 2022). However, the along-shelf pressure gradient term (estimated from tide gauges along the southern New England shelf) is as large as the terms in Eq. (3), and the along-shelf density gradient contribution to the pressure gradient may be

significant in summer (Lentz 2022). Including the along-shelf pressure gradient estimate [from Lentz (2022)] in the diagnostic model slightly improves the correlation between the model and the observed cross-shelf velocities—from 0.79 to 0.82 at 3 mab and from 0.82 to 0.85 at 3 m below the surface. These results provide further support for the idea that the cross-shelf circulation at monthly time scales is dominated by turbulent thermal-wind-driven upwelling (e.g., Fig. 10).

A key element of turbulent thermal-wind-driven upwelling that is not addressed in this study is the feedback between the upwelling circulation, the turbulent mixing, and the cross-shelf buoyancy (density) gradient that drives the upwelling circulation. It is clear in Fig. 1 that the upwelling circulation, in the absence of surface heating, would tend to reduce the cross-shelf density gradient, which, in turn, would reduce the upwelling circulation. As noted above, the offshore heat flux associated with the summer upwelling circulation tends to balance the incoming surface heat flux (Fewings and Lentz 2011). This suggests an equilibrium where the thermal-wind-driven upwelling circulation is just large enough to maintain a constant cross-shelf density gradient given the surface heat flux and/or the along-shelf freshwater flux. Such an equilibrium would depend not only on the buoyancy flux and inner-shelf geometry but also the turbulent stresses that are influenced by the density field. The remarkable consistency of the summer cross-shelf current profiles (Fig. 5a) suggests a robust equilibrium. Numerical model simulations are needed to determine if such an equilibrium exists and the characteristics of the feedback between the turbulence and the buoyancy forcing.

b. *Sources of cross-shelf density gradient and turbulent stresses*

The key elements in turbulent thermal-wind-driven coastal upwelling (or downwelling) are the cross-shelf density gradient that provides the buoyancy force that drives the cross-shelf circulation and turbulent stresses that allow release of the buoyancy force that would otherwise be in thermal-wind balance with the Coriolis force associated with the along-shelf velocity shear.

In the presence of strong surface heating or cooling cross-shelf temperature (and hence density) gradients may develop because of the order one variations in water depth across the inner shelf. The estimated cross-shelf temperature gradient at MVCO exhibits a seasonal cycle consistent with the surface heat flux and the decrease in water depth across the inner shelf. In summer (April–September), water temperatures increase toward shore (Fig. 13, blue circles), as expected for the strong surface heating in summer at this location (Fewings and Lentz 2011). In winter, water temperatures decrease toward shore as expected given the strong surface cooling (Connolly and Lentz 2014). The correlation between the cross-shelf temperature gradient and the surface heat flux is −0.9, primarily due to the annual cycle. The seasonal variation in the cross-shelf temperature gradient at MVCO is probably typical of many inner shelves with large seasonal variations in surface heat flux.

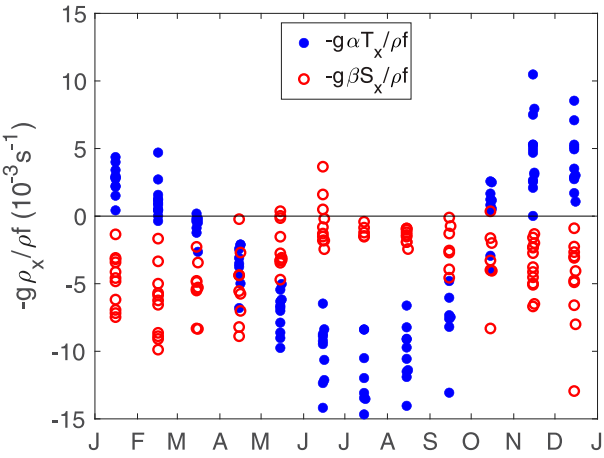

FIG. 13. The annual variation in estimates of the monthly cross-shelf temperature and salinity gradient contributions to the thermal-wind shear (see Fig. 6b for total).

In coastal regions with significant runoff, buoyant coastal currents are common over inner shelves and salinities typically decreases toward shore (e.g., Horner-Devine et al. 2015). This is the case at MVCO, where the cross-shelf salinity gradient is almost always positive with fresher (less dense) water nearer the coast (Fig. 13, red circles). The cross-shelf salinity gradient is relatively small in summer and larger in winter. The cause of this seasonal variation in the salinity gradient across the inner shelf is unclear (though see section 5c).

At MVCO the cross-shelf density gradient in summer (Figs. 1 and 6b) is almost entirely due to the cross-shelf temperature gradient (Fig. 13). In winter (October–December), the temperature and salinity gradients make similar contributions to the cross-shelf density gradient but typically have opposite signs, with salinity tending to dominate so that the cross-shelf density gradient generally remains positive (Fig. 6b). As discussed above, there is the potential for feedback that is not addressed in this study as the turbulent thermal-wind-driven upwelling circulation that is stronger in summer will impact both the cross-shelf temperature and salinity gradients.

Inner shelves are often defined as the region where surface and bottom boundary layers merge and hence turbulent stresses extend throughout the water column (e.g., Lentz and Fewings 2012). At MVCO winds and tidal currents tend to dominate the turbulent stresses that extend through the water column (Kirincich 2013). Tidal currents are particularly strong in this region (Shearman and Lentz 2004; He and Wilkin 2006; Kirincich et al. 2013) with along-shelf current magnitudes of 0.3 m s^{-1} at the 12-m site (Fewings et al. 2008). The strong tidal currents result in substantial bottom stresses (Scully et al. 2018) and turbulent stresses extending throughout most of the water column (Kirincich 2013). Wind stresses, particularly in winter, also drive substantial currents (Fewings et al. 2008; Horwitz and Lentz 2014) and turbulent stresses (Kirincich 2013). Bottom stresses are enhanced by surface gravity waves because there can be strong wave-orbital velocities near the bottom at this shallow site (Fewings and Lentz 2010; Scully et al. 2018; Lentz 2022).

Surface gravity waves also contribute to turbulence at the MVCO site through both wave breaking and Langmuir turbulence (Gerbi et al. 2009; Kukulka et al. 2011).

c. *Impact of turbulent thermal wind on coastal upwelling*

For the turbulent thermal-wind-driven upwelling in summer (Fig. 1), the flushing time for the volume onshore of the 12-m site is 2.5 days. (Flushing time is defined as cross-sectional area onshore of the 12-m site divided by the mean summer offshore transport seen in Fig. 1.) A consequence of this relatively short flushing time, in comparison with monthly time scales, is that the offshore heat flux associated with this upwelling circulation tends to balance the incoming surface heat flux in summer keeping the inner shelf at MVCO much cooler than it would be otherwise (Fewings and Lentz 2011). It also seems plausible that the reduced cross-shelf salinity gradient in summer is due to the persistent upwelling circulation. Salinities at MVCO are consistently lowest in July, presumably as a result of spring runoff from farther north. In the absence of any cross-shelf circulation, one might expect the cross-shelf salinity gradient to be largest when the salinity is lowest, which is opposite to what is observed.

Fewings and Lentz (2011) also note that there must be substantial advective cooling inshore of the 30-m isobath throughout the entire Middle Atlantic Bight (MAB) during the spring and early summer to account for the small increase in water temperature relative to the expected increase due to the surface heat flux. It seems plausible, if not likely, that turbulent thermal-wind-driven coastal upwelling contributes to the required advective cooling throughout the MAB. While direct evidence in support of this hypothesis is lacking at present, there is a mean upwelling circulation on the New Jersey inner shelf (LEO-15 site) that is nearly identical to the mean upwelling circulation at MVCO (Fig. 6a in Lentz 2008). At monthly time scales, there is also a persistent upwelling circulation over the inner shelf near the mouth of Long Island Sound (Ullman and Codiga 2004), although it is unclear whether this is due to a turbulent thermal-wind balance given the complexity of the flow in this region.

The persistent upwelling circulation may be an important source of nutrients to near-surface waters over the inner shelf. However, this clearly depends on whether the turbulent thermal driven upwelling extends deep enough to provide a significant nutrient flux. The persistence and consistency of the upwelling circulation also provides an extremely reliable mechanism for larval transport across the inner shelf in the vicinity of MVCO.

A key set of questions that are not addressed in this study is how turbulent thermal-wind-driven upwelling over the inner shelf impacts and is impacted by the stratified midshelf offshore and the more energetic surfzone onshore. Turbulent thermal-wind-driven coastal upwelling should be limited to the inner shelf where turbulent mixing extends throughout the water column. How far offshore this coastal upwelling extends is an important, unresolved question. The analyses of Fewings and Lentz (2011) suggest it may be limited to onshore of about the 30-m isobath, at least in the Middle Atlantic Bight. Recent studies have demonstrated the importance of surfzone eddies and transient rip currents to exchange between the surfzone and the inner shelf (e.g., Clark et al. 2011; Hally-Rosendahl et al. 2014; Kumar and Feddersen 2017a). It is unclear how transient rip currents impact the development of turbulent thermal-wind-driven exchange near the surfzone and how these two processes interact to determine exchange between the surfzone and the inner shelf. This is particularly interesting because modeling studies of transient rip current exchange with a stratified inner shelf have shown the development of a thermal-wind balance offshore of the surfzone (Kumar and Feddersen 2017b).

6. Summary

Seventeen years of current profiles in 12 m of water from the Martha's Vineyard Coastal Observatory provide a rare opportunity to examine the characteristics and dynamics of the cross-shelf circulation over an inner shelf. There is a depth-average offshore transport that is roughly equal in magnitude but opposite in direction to the onshore Stokes transport (Fig. 4), consistent with previous studies focusing on daily time scales (e.g., Lentz et al. 2008). Cross-shelf wind stresses also force significant cross-shelf circulations (Fig. 12), particularly in winter, again consistent with previous studies focusing on daily time scales (Fewings et al. 2008; Horwitz and Lentz 2014). However, the dominant cross-shelf circulation is a remarkably consistent upwelling circulation at monthly and longer time scales, which is not obvious at shorter time scales. During the summer months (April–September), the mean Lagrangian cross-shelf current (depth-average removed) is ~1 cm s^{-1} offshore at 3 m below the surface and 1 cm s^{-1} onshore flow at 3 m above the bottom (Figs. 1, 5a, and 6a). At monthly time scales both interannual and intraseasonal variations from the mean summer upwelling circulation are small, standard deviations of 0.2 cm s^{-1} or less at all depths. In winter (October–March), the mean Lagrangian upwelling circulation is weaker, about half the summer magnitude, but the variations are larger with occasionally a weak downwelling circulation in November and December (Figs. 5b and 6a). A small fraction of the month-to-month variability in the cross-shelf circulation, particularly in winter, is driven by cross-shelf wind stresses (Fig. 9).

The persistent upwelling circulation, the annual cycle, and most of the month-to-month variability is not wind-driven and seems inconsistent with the mean westward (downwelling-favorable) along-shelf current at this site (note isopycnals tilting downward toward coast in Fig. 1). The observed upwelling circulation is driven by the buoyancy force associated with a cross-shelf density gradient with lighter water near the coast. The density gradient is primarily due to temperature in summer when strong surface heating warms shallower nearshore water more than deeper offshore water (Fig. 13). In winter, there is a stronger salinity gradient with fresher water near the coast that tends to be larger than the opposing temperature gradient contribution to density caused by surface cooling. In the absence of turbulent stresses, the cross-shelf density gradient would be in a geostrophic,

thermal-wind balance with the vertical shear in the alongshelf current. However, turbulent stresses over the inner shelf due to tidal currents and wind stress cause a partial breakdown of the thermal-wind balance (Figs. 6b,c and 7). The resulting net buoyancy force drives an upwelling circulation with lighter water flowing offshore in the upper half of the water column and denser water flowing onshore in the lower half of the water column (Fig. 1). The key result of this study is that the presence of a cross-shelf density gradient can have a profound impact on exchange across the inner shelf (Fig. 10). Most inner shelves are characterized by cross-shelf density gradients with lighter water near the coast and turbulent stresses suggesting turbulent thermal-wind-driven coastal upwelling (or downwelling) may be a broadly important cross-shelf exchange mechanism.

Acknowledgments. This study is possible because of all the people that contributed to the Martha's Vineyard Coastal Observatory, including deploying and maintaining the instrumentation and processing and archiving the resulting data. Anthony Kirincich, Ken Brink, Falk Feddersen, and an anonymous reviewer made numerous suggestions that substantially improved this paper. The National Science Foundation, Woods Hole Oceanographic Institution, the Massachusetts Technology Collaborative, and the Office of Naval Research have supported the construction and maintenance of MVCO. The analysis presented here was partially funded by the National Science Foundation under Grants OCE 1558874 and OCE 1655686.

Data availability statement. The MVCO data are available online (https://mvco.whoi.edu), as are the data from the SWWIM field program (https://hdl.handella33le.net/1912/27252).

REFERENCES

Brink, K. H., 2016: Cross-shelf exchange. *Annu. Rev. Mar. Sci.*, **8**, 59–78, https://doi.org/10.1146/annurev-marine-010814-015717.

——, R. C. Beardsley, R. Limeburner, J. D. Irish, and M. Caruso, 2009: Long-term moored array measurements of currents and hydrography over Georges Bank: 1994–1999. *Prog. Oceanogr.*, **82**, 191–223, https://doi.org/10.1016/j.pocean.2009.07.004.

Chen, S.-Y., and S.-N. Chen, 2017: Generation of upwelling circulation under downwelling-favorable wind within bottom-attached, buoyant coastal currents. *J. Phys. Oceanogr.*, **47**, 2499–2519, https://doi.org/10.1175/JPO-D-16-0271.1.

Clark, D. B., F. Feddersen, and R. T. Guza, 2011: Modeling surfzone tracer plumes: 2. Transport and dispersion. *J. Geophys. Res.*, **116**, C11028, https://doi.org/10.1029/2011JC007210.

Connolly, T. P., and S. J. Lentz, 2014: Interannual variability of wintertime temperature on the inner continental shelf of the middle Atlantic bight. *J. Geophys. Res. Oceans*, **119**, 6269–6285, https://doi.org/10.1002/2014JC010153.

Edson, J. B., and Coauthors, 2013: On the exchange of momentum over the open ocean. *J. Phys. Oceanogr.*, **43**, 1589–1610, https://doi.org/10.1175/JPO-D-12-0173.1.

Ekman, V. W., 1905: On the influence of the Earth's rotation on ocean-currents. *Ark. Mat. Aston. Fys.*, **2**, 1–53.

Falkowski, P. G., R. T. Barber, and V. Smetacek, 1998: Biogeochemical controls and feedbacks on ocean primary production. *Science*, **281**, 200–206, https://doi.org/10.1126/science.281.5374.200.

Fewings, M. R., and S. J. Lentz, 2010: Momentum balances on the inner continental shelf at Martha's Vineyard coastal observatory. *J. Geophys. Res.*, **115**, C12023, https://doi.org/10.1029/2009JC005578.

——, and ——, 2011: Summertime cooling of the shallow continental shelf. *J. Geophys. Res.*, **116**, C07015, https://doi.org/10.1029/2010JC006744.

——, ——, and J. Fredericks, 2008: Observations of cross-shore flow driven by cross-shore winds on the inner continental shelf. *J. Phys. Oceanogr.*, **38**, 2358–2378, https://doi.org/10.1175/2008JPO3990.1.

Garrett, C. J., and J. W. Loder, 1981: Dynamical aspects of shallow sea fronts. *Philos. Trans. Roy. Soc.*, **A302**, 563–581, https://doi.org/10.1098/rsta.1981.0183.

Gerbi, G. P., J. H. Trowbridge, E. A. Terray, A. J. Plueddemann, and T. Kukulka, 2009: Observations of turbulence in the ocean surface boundary layer: Energetics and transport. *J. Phys. Oceanogr.*, **39**, 1077–1096, https://doi.org/10.1175/2008JPO4044.1.

Grimes, D. J., F. Feddersen, and N. Kumar, 2020: Tracer exchange across the stratified inner-shelf driven by transient rip-currents and diurnal surface heat fluxes. *Geophys. Res. Lett.*, **47**, e2019GL086501, https://doi.org/10.1029/2019GL086501.

Gula, J., M. J. Molemaker, and J. C. McWilliams, 2014: Submesoscale cold filaments in the Gulf Stream. *J. Phys. Oceanogr.*, **44**, 2617–2643, https://doi.org/10.1175/JPO-D-14-0029.1.

Hally-Rosendahl, K., F. Feddersen, and R. T. Guza, 2014: Cross-shore tracer exchange between the surfzone and inner-shelf. *J. Geophys. Res. Oceans*, **119**, 4367–4388, https://doi.org/10.1002/2013JC009722.

He, R., and J. H. Wilkin, 2006: Barotropic tides on the southeast New England shelf: A view from a hybrid data assimilative modeling approach. *J. Geophys. Res.*, **111**, C08002, https://doi.org/10.1029/2005JC003254.

Heaps, N. S., 1972: Estimation of density currents in the Liverpool Bay area of the Irish Sea. *Geophys. J. Int.*, **30**, 415–432, https://doi.org/10.1111/j.1365-246X.1972.tb05825.x.

Horner-Devine, A. R., R. D. Hetland, and D. G. MacDonald, 2015: Mixing and transport in coastal river plumes. *Annu. Rev. Fluid Mech.*, **47**, 569–594, https://doi.org/10.1146/annurev-fluid-010313-141408.

Horwitz, R., and S. J. Lentz, 2014: Inner-shelf response to cross-shelf wind stress: The importance of the cross-shelf density gradient in an idealized numerical model and field observations. *J. Phys. Oceanogr.*, **44**, 86–103, https://doi.org/10.1175/JPO-D-13-075.1.

James, I. D., 1978: A note on the circulation induced by a shallow-sea front. *Estuarine Coastal Mar. Sci.*, **7**, 197–202, https://doi.org/10.1016/0302-3524(78)90075-0.

Kenyon, K. E., 1969: Stokes drift for random gravity waves. *J. Geophys. Res.*, **74**, 6991–6994, https://doi.org/10.1029/JC074i028p06991.

Kirincich, A. R., 2013: Long-term observations of turbulent Reynolds stresses over the inner continental shelf. *J. Phys. Oceanogr.*, **43**, 2752–2771, https://doi.org/10.1175/JPO-D-12-0153.1.

——, 2016: The occurrence, drivers, and implications of submesoscale eddies on the Martha's Vineyard inner shelf. *J. Phys.*

Oceanogr., **46**, 2645–2662, https://doi.org/10.1175/JPO-D-15-0191.1.

——, 2021: Martha's Vineyard Coastal Observatory 2021: State of the observatory report. Woods Hole Oceanographic Institution Rep., 40 pp., https://www.whoi.edu/wp-content/uploads/2021/08/MVCO2021.pdf.

——, and S. J. Lentz, 2017: The importance of lateral variability on exchange across the inner shelf south of Martha's Vineyard, MA. *J. Geophys. Res. Oceans*, **122**, 2360–2381, https://doi.org/10.1002/2016JC012491.

——, ——, and J. A. Barth, 2009: Wave-driven inner-shelf motions on the Oregon coast. *J. Phys. Oceanogr.*, **39**, 2942–2956, https://doi.org/10.1175/2009JPO4041.1.

——, ——, J. T. Farrar, and N. K. Ganju, 2013: The spatial structure of tidal and mean circulation over the inner shelf south of Martha's Vineyard, Massachusetts. *J. Phys. Oceanogr.*, **43**, 1940–1958, https://doi.org/10.1175/JPO-D-13-020.1.

Kukulka, T., A. J. Plueddemann, J. H. Trowbridge, and P. P. Sullivan, 2011: The influence of crosswind tidal currents on Langmuir circulation in a shallow ocean. *J. Geophys. Res.*, **116**, C08005, https://doi.org/10.1029/2011JC006971.

Kumar, N., and F. Feddersen, 2017a: A new offshore transport mechanism for shoreline-released tracer induced by transient rip currents and stratification. *Geophys. Res. Lett.*, **44**, 2843–2851, https://doi.org/10.1002/2017GL072611.

——, and ——, 2017b: The effect of Stokes drift and transient rip currents on the inner shelf. Part II: With stratification. *J. Phys. Oceanogr.*, **47**, 243–260, https://doi.org/10.1175/JPO-D-16-0077.1.

Lentz, S. J., 1995: Sensitivity of the inner-shelf circulation to the form of the eddy viscosity profile. *J. Phys. Oceanogr.*, **25**, 19–28, https://doi.org/10.1175/1520-0485(1995)025<0019:SOTISC>2.0.CO;2.

——, 2008: Observations and a model of the mean circulation over the middle Atlantic bight continental shelf. *J. Phys. Oceanogr.*, **38**, 1203–1221, https://doi.org/10.1175/2007JPO3768.1.

——, 2022: Interannual and seasonal along-shelf current variability and dynamics—Seventeen years of observations over the southern New England inner shelf. *J. Phys. Oceanogr.*, **52**, 2923–2933, https://doi.org/10.1175/JPO-D-22-0064.1.

——, and M. R. Fewings, 2012: The wind-and wave-driven inner-shelf circulation. *Annu. Rev. Mar. Sci.*, **4**, 317–343, https://doi.org/10.1146/annurev-marine-120709-142745.

——, ——, P. Howd, J. Fredericks, and K. Hathaway, 2008: Observations and a model of undertow over the inner continental shelf. *J. Phys. Oceanogr.*, **38**, 2341–2357, https://doi.org/10.1175/2008JPO3986.1.

Loder, J. W., and D. G. Wright, 1985: Tidal rectification and frontal circulation on the sides of Georges Bank. *J. Mar. Res.*, **43**, 581–604, https://doi.org/10.1357/002224085788440367.

McWilliams, J. C., and E. Huckle, 2006: Ekman layer rectification. *J. Phys. Oceanogr.*, **36**, 1646–1659, https://doi.org/10.1175/JPO2912.1.

——, J. Gula, M. J. Molemaker, L. Renault, and A. F. Shchepetkin, 2015: Filament frontogenesis by boundary layer turbulence. *J. Phys. Oceanogr.*, **45**, 1988–2005, https://doi.org/10.1175/JPO-D-14-0211.1.

Moffat, C., and S. Lentz, 2012: On the response of a buoyant plume to downwelling-favorable wind stress. *J. Phys. Oceanogr.*, **42**, 1083–1098, https://doi.org/10.1175/JPO-D-11-015.1.

Nagai, T., A. Tandon, and D. Rudnick, 2006: Two-dimensional ageostrophic secondary circulations at ocean fronts due to vertical mixing and large-scale deformation. *J. Geophys. Res.*, **111**, C09038, https://doi.org/10.1029/2005JC002964.

Pawlowicz, R., B. Beardsley, and S. Lentz, 2002: Classical tidal harmonic analysis including errors in MATLAB using T_TIDE. *Comput. Geosci.*, **28**, 929–937, https://doi.org/10.1016/S0098-3004(02)00013-4.

Ponte, A. L, P. Klein, X. Capet, P.-Y. Le Traon, B. Chapron, and P. Lherminier, 2013: Diagnosing surface mixed layer dynamics from high-resolution satellite observations: Numerical insights. *J. Phys. Oceanogr.*, **43**, 1345–1355, https://doi.org/10.1175/JPO-D-12-0136.1.

Scully, M. E., J. H. Trowbridge, C. R. Sherwood, K. R. Jones, and P. Traykovski, 2018: Direct measurements of mean Reynolds stress and ripple roughness in the presence of energetic forcing by surface waves. *J. Geophys. Res. Oceans*, **123**, 2494–2512, https://doi.org/10.1002/2017JC013252.

Shearman, R. K., and S. J. Lentz, 2004: Observations of tidal variability on the New England Shelf. *J. Geophys. Res.*, **109**, C06010, https://doi.org/10.1029/2003JC001972.

Smith, R. L., 1981: A comparison of the structure and variability of the flow field in three coastal upwelling regions: Oregon, Northwest Africa, and Peru. *Coastal Upwelling*, F. A. Richards, Ed., Coastal and Estuarine Sciences Series, Vol. 1, Amer. Geophys. Union, 107–118.

Tilburg, C., 2003: Across-shelf transport on a continental shelf: Do across-shelf winds matter? *J. Phys. Oceanogr.*, **33**, 2675–2688, https://doi.org/10.1175/1520-0485(2003)033<2675:ATOACS>2.0.CO;2.

Ullman, D. S., and D. L. Codiga, 2004: Seasonal variation of a coastal jet in the Long Island Sound outflow region based on HF radar and Doppler current observations. *J. Geophys. Res.*, **109**, C07S06, https://doi.org/10.1029/2002JC001660.

Ulloa, H. N., K. A. Davis, S. G. Monismith, and G. Pawlak, 2018: Temporal variability in thermally driven cross-shore exchange: The role of semidiurnal tides. *J. Phys. Oceanogr.*, **48**, 1513–1531, https://doi.org/10.1175/JPO-D-17-0257.1.

Webb, A., and B. Fox-Kemper, 2015: Impacts of wave spreading and multidirectional waves on estimating Stokes drift. *Ocean Modell.*, **96**, 49–64, https://doi.org/10.1016/j.ocemod.2014.12.007.